ORIGINAL RESEARCH (AR) DOI: 10.4274/jems.2024.67689

Journal of ETA Maritime Science 2024;12(3):332-345

Combined Effects of Axial Flow and High System Rotation on the Fluid Dynamics of Taylor-Couette-Poiseuille Flow

Taner Çoşgun, Nurten Vardar

Yıldız Technical University Faculty of Naval Arthitecture and Maritime, Department of Naval Architecture and Marine Engineering, İstanbul, Türkiye

Abstract

Taylor-Couette-Poiseuille (TCP) flow, characterized by the flow through an inner rotating shaft and an outer stationary cylinder, is a fundamental flow system in many industrial applications, including ship stern tubes, turbomachinery, journal bearings, and offshore drilling. Understanding the hydrodynamics of the TCP flow offers significant benefits for ensuring the robust design and operational efficiency of such systems. This paper presents the numerical modeling of turbulent TCP flow to assess the combined effects of two key control parameters-axial Reynolds number (10000-30000) and Taylor number ($2.2x10^7$-$3.1x10^9$)-on the fluid dynamics within the system. Using Reynolds Stress Modeling, this study investigates the behavior of TCP flow at high Reynolds numbers, which is relevant to real-world rotating machinery. The results indicate that the interaction between rotation and axial flow is not linear, with high rotation rates showing distinct behavior from low rotation rates, especially in the throughflow effects. At low and moderate rotation numbers (N), both the mean and turbulent variables display strong dependence on the rotational velocity and axial flow rate. However, further increases in N lead the flow field to be increasingly dominated by the contribution of rotation, and mean flow variables become relatively independent of the imposed flow rate. Furthermore, systematic deviations from the log-law in the boundary layer velocity profiles further emphasize the need to account for the combined effects of rotation and axial flow in the TCP flow system design and operation.

Keywords: Taylor-Couette-Poiseuille flow, Annular flow, Turbulence, Computational fluid dynamics, Concentric annulus, Stern tube

1. Introduction

The flow within the annular cavity between rotating concentric cylinders, also known as Taylor-Couette (TC) flow, is a great area of interest in fluid dynamics research. Beyond its role as a fundamental flow system in many industrial applications [1,2], TC flow can also serve as an important test case in turbulent flow studies [3].

TC flow is a closed system in which a moving cylinder wall creates flow within the cavity. Introducing an axial flow to an open-ended TC system creates a configuration known as Taylor-Couette-Poiseuille (TCP) flow. The presence of axial flow significantly complicates the fluid behavior by adding a second key parameter (throughflow) that influences the flow field [4]. In such a flow, the balance between the additional body forces induced by inner cylinder rotation and the pressure-driven axial flow is shaped by the flow field dynamics. The arrangement of concentric rotating cylinders is a common feature in various engineering applications, including ship stern tubes, journal bearings, turbomachinery, cooling systems for electrical devices, drilling operations, and fluid filtration devices… etc. Therefore, a deeper understanding of the TCP flow field is beneficial not only for the theory of turbulent flow in rotating systems but also for the reliable design and operation of such systems.

The superposition of the axial and rotational flows in the TCP system is not a linear combination of TC and annular Poiseuille flows; thus, each pair of axial rotational velocities induces a different flow field. In other words, the characteristics of the turbulent flow field can vary between canonical flows. The influence of two main flow parameters (rotational and axial velocities) on the features of the turbulence has already

Address for Correspondence: Taner Çoşgun, Yıldız Technical University Faculty of Naval Arthitecture and Maritime, Department of Naval Architecture and Marine Engineering, İstanbul, Türkiye
E-mail: tcosgun@yildiz.edu.tr
ORCID iD: orcid.org/0000-0002-1364-0133

Received: 13.06.2024
Last Revision Received: 22.07.2024
Accepted: 03.08.2024

To cite this article: T. Çoşgun, and N. Vardar. "Combined Effects of Axial Flow and High System Rotation on the Fluid Dynamics of Taylor-Couette-Poiseuille Flow." *Journal of ETA Maritime Science*, vol. 12(3), pp. 332-345, 2024.

been motivated by several studies. Nouri and Whitelaw [5] experimentally measured the mean velocities and turbulence stresses of a flow in a concentric annulus with a rotating inner cylinder. They observed an enhancement of the turbulence statistics with inner wall rotation compared to those of the non-rotating case. They also concluded that the same rotation rates of the inner cylinder affected the flow field, depending on whether the imposed axial flow was laminar or turbulent. Escudier and Coulson [6] investigated the TCP flow in a similar experimental arrangement. Their results emphasized that an increase in axial Re diminishes the magnitude of the tangential velocity of inner cylinder rotation, especially in the central region of the annulus. Also, the turbulence fluctuations are suppressed at higher axial flow rates. Chung et al. [7] applied direct numerical simulation to the flow through an annular gap between concentric cylinders without inner wall rotation. They reported that the annular flow between concentric pipes has the general characteristics of fully developed internal flows like channel and pipe flows. At a later date, they performed a large-eddy simulation (LES) to examine the effects of inner cylinder rotation under the same geometrical configuration and axial flow conditions [8]. They showed an increase in the overall turbulence statistics with inner wall rotation. They found that the flow became more isotropic, and the increasing tendency of the turbulence statistics was more apparent at high rotation rates. The authors addressed the destabilizing effect of inner wall rotation on the alteration of the turbulent field. Liu and Lu [9] investigated the near-wall turbulence features of both stationary and moving walls in TCP flows. Jung and Sung [10] conducted direct numerical simulations to examine the turbulent boundary layers in a concentric annulus with a rotating inner wall. They clarified the modifications in the near-wall turbulent structures with the centrifugal force induced by the rotation of the inner cylinder. Hadžiabdić et al. [11] studied the effect of outer cylinder rotation in an annular flow. They revealed that the variation trend of the turbulence features with increasing rotational wall velocity can be reversed after a critical value of rotation number. They also used the Ta/Re2 ratio as a dynamic representative of the ratio of the centrifugal to axial inertial forces, instead of the rotation number Poncet et al. [12] studied the TCP flow in a narrow gap cavity with six different combinations of axial and rotational flow conditions using an LES. They found that inner wall rotation dominated the mean tangential velocity profile, and the fluid rotated nearly in solid body rotation, especially in the core region. In addition, turbulence is mostly concentrated in the boundary layers.

Due to the significant resemblance of TCP flow to many engineering systems, investigations of hydrodynamic features like skin friction, rotating cylinder torque, pressure drop, and heat transfer are important for industrial applications. Thus, several researchers have focused on such hydrodynamic properties in TCP flows. Yamada [13] measured the resistance of an annular flow with a rotating inner cylinder. Their results showed that lowers the inner cylinder resistance to a certain level, while a further increase in Re raises the resistance. Manna and Vacca [14] numerically investigated the torque reduction behavior under a superimposed axial pressure gradient in a TCP flow. A detailed flow field analysis in the study indicates that the torque reduction is associated with the modification of the large-scale coherent structures, as imposed by the axial flow. Oshawa et al. [15] investigated the contributions of Reynolds stress terms to torque variations under diabatic conditions. The experimental study by Woo et al. [16] showed that the pressure loss of TCP flow increases with inner cylinder rotation. Chong et al. [17] measured the pressure drop in an annular passage with a rotating inner cylinder to investigate the flow entry effects in the rotor-stator gap of electrical machines. Various authors have investigated the heat transfer mechanism in TCP flow including [18-22]. A review of heat transfer studies can be found in the extended literature review by Fénot et al. [4]. They concluded that more data on the hydrodynamic field should be provided to eliminate the many question marks concerning TCP heat transfer.

The literature review reveals that TCP flow has been exhaustively studied over the last few decades. Table 1 summarizes the primary findings and investigated ranges of the relevant literature. It can be seen that most previous research, especially those focused on the hydrodynamic and turbulent fields, considered relatively lower rotation numbers. The parameter range in some heat transfer studies can reach higher values, but they are generally focused on the measurement/prediction of the thermal field. Reference [4] highlighted the importance of understanding the flow physics associated with TCP heat transfer. On the other hand, under real operating conditions in industrial applications, very high rotational and axial velocities. Poncet et al. [12,19] pointed out the need for reliable data at high rotation rates, which is also the motivation of the present work. The last author performed numerical simulations to understand the hydrodynamical behavior and heat transfer under the real operating conditions of electrical machinery. Nevertheless, their studies concerned a narrow gap cavity and gap height, which play important roles in the dynamics of annular flows [7,23]. The purpose of the present study was to investigate the mean and turbulent field in a middle-gap TCP flow over a wide range of rotational numbers from low to very high. The 15 different combinations of rotational and axial velocities in the parameter space of the study provided a rich data field to examine the fluid dynamics of the system. The second aim of this work was to study the effects of superimposed axial flow at high system rotation.

Table 1. *Summary of relevant literature in the investigated ranges. Throughout the literature, scaling the system rotation does not have unity in both the selection of the parameter that is used to quantify the rotational velocity of the inner cylinder and the definition of that parameter itself. In addition, it is not possible to convert them to a single parameter. Hence, the flow control parameters of the summarized papers are presented in the following sections. The parameter range of the present study is 10000-30000 for axial Reynolds number and $2.2x10^7$-$3.1x10^9$ for Taylor Number.*

Ref.	Type	r	Axial flow parameters	Range	Rotational flow parameter	Range	Primary findings
[24]	Exp.	0.8	$Re = 2sU/\nu$	0-12000	$Ta = \frac{\omega^2 r_m (r_o - r_i)^3}{\nu^2}$	0-330000	Temperature measurements over a wide range of flow parameters. A regimen map is created for diabatic and adiabatic flows.
[13]	Exp.	0.89-0.98	$Re = sU/\nu$	0-30000	$Re_\omega = \omega R_i s / \nu$	0-30000	Flow resistance measurements at six gap heights and various combinations of axial and rotational velocities. The friction coefficient was found to be unaffected when the axial flow was laminar. Beyond a certain level of rotational velocity the resistance increases.
[25]	Exp./ Num.	0.5	$Re = sU/\nu$	0- 150	$Ta = \omega s^2 / \nu$	0-170	The linear stability of the spiral flow was investigated. The observed critical Taylor numbers were compared with the theoretical predictions.
[26]	Exp.	0.71	$Re = 2sU/\nu$	0-137	$Ta = \frac{(\omega r_i^{1/2} s^{3/2} / \nu)}{1.43}$	255	Visual observations of the vortex structure. Complete vortex destruction after Re/Ta > 0.55
[27]	Exp.	0.8	$Re = 2sU/\nu$	500-1250	$Ta = \omega R_i s / \nu$	0-500	The heat and mass transfer observations were performed. The mass transfer coefficients were enhanced at high rotational velocities.
[28]	Exp.	0.85	$Re = 2sU/\nu$	0-37	$Ta = \omega R_i s / \nu$	0-2900	Seven intermediary flow regimes were identified by optical techniques. A stability map for the TCP flow is generated.
[5]	Exp.	0.5	$Re = 2sU/\nu$	950, 9000, 26600	rpm/ $Re_\omega = \omega R_i s / \nu$	0,300/ 0,398	Mean flow and Reynolds stresses in Newtonian and non-Newtonian fluids. Turbulence enhancement is observed with rotation.
[6]	Exp.	0.5	$Re = 2sU/\nu$	1200, 2700, 7400	rpm/ $Ta = (\omega / \nu)^2 r_i s^3$	126/ $8.78x10^5$	LDA measurements of mean flow and Reynolds stresses in Newtonian and shear-thinning fluids. An increase in the axial flow reduces the mean tangential velocity and fluctuations.
[29]	Exp.	0.83	$Re = sU/\nu$	1.6-23	$Ta = \omega R_i s / \nu$	100-215	PIV measurements in the meridional plane of the annulus. The vortex behavior was investigated in detail at low axial flow rates.
[30]	Num.	0.83	$Re = sU/\nu$	1.6-23	$Ta = \omega R_i s / \nu$	100-215	Experimental stability analysis of (Wereley & Lueptow, 1999) was numerically validated. The axial flow stabilizes the flow field and reduces the torque coefficient on the inner cylinder.
[8]	Num.	0.5	$Re = 2sU/\nu$	8900	$N = V_\theta / U$	0.214, 0.429, 0.858	Destabilization of the near-wall turbulent structures due to the rotation of the inner cylinder was revealed using the LES. Various turbulence statistics were investigated.

Table 1. Continued

Ref.	Type	r	Axial flow parameters	Range	Rotational flow parameter	Range	Primary findings
[9]	Num.	0.5	$\mathrm{Re} = sU_\tau/\nu$	640	$N = 2\omega s / U$	0-20	The turbulence statistics and TKE budget in the TCP flow were investigated in detail using the LES. Significant change in the radial and azimuthal turbulence intensities with rotation, as well as an increasing Coriolis term in the TKE budget.
[16]	Exp.	0.52	$\mathrm{Re} = 2sU/\nu$	100-12000	rpm	0-600	Pressure losses and skin friction coefficients were measured for water and non-Newtonian fluids. Critical Re was found to decrease with increasing rotation rate, whereas the pressure loss increased.
[31]	Num.	0.5	$\mathrm{Re} = 2sU/\nu$	8900	$N = U_\theta / U$	0.171, 0.257	The combined effects of buoyancy and inner wall rotation on the mixed convection in TCP flow were demonstrated. Rotation suppresses the heat-reducing effects on the turbulence statistics.
[32]	Exp.	0.9	$\mathrm{Re} = sU/\nu$	30-1200	$\mathrm{Re}_\omega = \omega R_i s / \nu$	0-2922	The effect of longitudinal ribs mounted on the rotating inner cylinder on the heat transfer characteristics of TCP was investigated. Significant heat transfer enhancement was observed with ribs.
[14]	Num.	0.98	$\mathrm{Re} = sU/\nu$	0-400	$Ta = \omega R_i s / \nu$	1000-15000	The torque reduction behavior at low axial velocities was confirmed using DNS. The relationship between torque reduction and large-scale coherent structures was revealed.
[19]	Num.	0.96	$C_W = Q/\nu r_o$	0-30000	$\mathrm{Re}_i = \omega R_i s / \nu$	3744-37443	The effects of flow parameters on heat transfer characteristics are presented. Correlations for the averaged Nusselt numbers along both cylinders are provided.
[33]	Exp.	0.99	$\mathrm{Re} = 2sU/\nu$	2140-6425	$\mathrm{Re}_r = V_r s / \nu$	1750-35000	Heat transfer in a TCP system with a slotted inner cylinder is investigated. The importance of the axial ratio and entrance velocity profile on heat transfer is presented.
[11]	Num.	0.5	$\mathrm{Re} = 2sU/\nu$	12500	$N = U_\theta / U$	0.5- 4	LES modeling of the influence of outer cylinder rotation. A critical N was determined at which the effect of rotation on turbulence is reversed.
[34]	Num.	0.5, 0.89	$\mathrm{Re} = sU/\nu$	50-200	$\mathrm{Re}_\omega = \omega R_i s / \nu$	127-296	The combined effects of eccentricity and axial velocity on the TCP stability were investigated. Eccentricity stabilizes the system regardless of the axial flow rate.

Table 1. Continued

Ref.	Type	r	Axial flow parameters	Range	Rotational flow parameter	Range	Primary findings
[12]	Num.	0.88	$Re = sU/\nu$	3745, 5617	$N = Re_\Omega / Re_a$ $(N = \omega R_i / U)$	2.24-4.47	Investigation of mean flow, turbulent field, and near-wall flow in a wide range of flow parameters using LES. The boundary layers along the inner and outer walls are governed by the effective Re and are found to be two-dimensional. The non-isothermal case was also studied.
[20]	Exp.	0.88	$Re = 2sU/\nu$	7490-11200	$Ta = \omega^2 R_i s^3 / \nu^2$	$8.8x10^6$-$7.9x10^7$	Velocity and temperature measurements over a wide range of flow parameters. A correlation is provided for the Nusselt number on the rotating wall.
[35]	Exp./ Num.	0.78	$Re = sU/\nu$	7589	$Ta = \omega^2 R_i s^3 / \nu^2$	$3.2x10^8$	Heat transfer and power loss (drag force) were studied at high rotation speeds. RANS methodology. Nusselt number correlation was proposed.
[36]	Exp.	0.85	$Re = 2sU/\nu$	1.49-120	$Ta = \frac{\omega r_i s}{\nu}\sqrt{\frac{s}{r_i}}$	46-680	PIV investigation of the vortex field. Vortex formation under different flow conditions was demonstrated.
[21]	Num.	0.5	$Re = 2sU/\nu$	9000	$N = \omega R_i / U$	0.21, 0.86	The influence of rotation on heat transfer in the TCP flow was also investigated. The destabilizing effect of rotation enhances mixing and Nusselt number.
[37]	Num.	0.85	$\beta = sU/\nu$	0-40	$Ta = \omega R_i s / \nu$	110-150	Stability analysis of TCP flow on permeable surfaces using DNS. Three different configurations were tested: radial flow injection, extraction, and cross-flow.
[38]	Num.	0.77	$Re = sU/\nu$	1500, 7500	$Re_t = \omega R_i s / \nu$	$3.7x10^4$-$1.5x10^5$	The effect of contracting the outer cylinder on the pressure field was investigated. Counter-rotating Taylor vortex pairs cause pressure oscillations. A prediction model was developed.
[39]	Num.	0.93	$Re = d_h U/\nu$	5000-65000	$Re_t = \omega R_i d_h / \nu$	160-1900	The thermal performance of various outer cylinder shapes was investigated. Heat transfer characteristics and pressure drop values were obtained for three cavity shapes.
[40]	Num.	0.8	$Re = 2sU/\nu$	2100-2400	$Ta_m = \frac{\omega^2 R_m s^3}{\nu F_g}$	30000-90000	Thermal performance analysis of the TCP flow with longitudinal and helical ribs mounted on the inner cylinder. Ribs induce more vorticity and turbulence and enhance heat transfer.
[41]	Num.	0.83	$Re = 2sU/\nu$	730-14600	$Ta = \omega^2 R_i s^3 / \nu^2$	10^5-10^9	The effect of the imposed radial flow through the inner cylinder surface on heat transfer was investigated. The thermal efficiency of the radial flow case was superior to that of the axial flow case.
[42]	Num.	0.5	$Re = 2sU/\nu$	10000	$N = U_\theta / U$	0-4	Numerical predictions were performed using the LES and RANS methodologies. The effects of high rotation rates on the turbulence statistics and mean flow were investigated.

With this object in mind, the same set of rotational parameters was tested for different axial Reynolds numbers. Thus, numerical results were presented separately in terms of rotation and axial velocity to observe the effects of varying operating conditions on the mean flow features, turbulent field, and boundary layer structure.

2. Numerical Modeling

2.1. Geometry and Flow Conditions

Figure 1 shows the schematic view of the TCP flow configuration. The solution domain is composed of a stationary outer cylinder with radii r_o and an inner cylinder with radii r_i which is rotating around its axis with constant angular velocity ω. The radius ratio of the cylinders is r_i/r_o=0.506. The cavity length in the streamwise direction is L=10s (where $s = r_0 - r_i$).

Three values of the axial velocity and five values of the rotation rate of the inner cylinder were considered in this study.

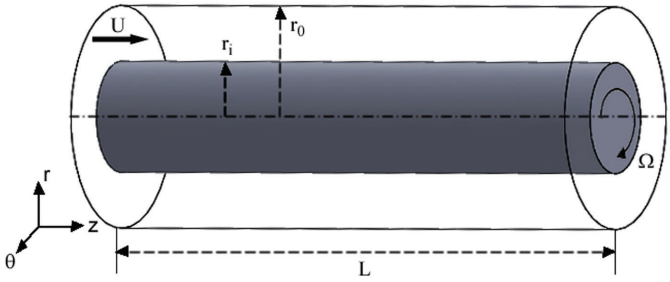

Figure 1. *Schematic of the problem*

The ranges of the flow control parameters are given in Table 2. The assumed throughflow is characterized by the axial Reynolds number based on the hydraulic diameter, $\mathrm{Re} = 2sU/\nu$, where U is the bulk velocity at the inlet and ν is the kinematic viscosity. The rotational Reynolds number, $\mathrm{Re}_\omega = \omega r_i s/\nu$, donates the rotating velocity of the inner wall. The equivalent Taylor number Ta and rotation number N are also given in Table 2, for comparison with similar studies. The Taylor number is defined as $Ta = \omega^2 r_i s^3/\nu^2$ and the rotation number is $N = U_\Omega/U$, where $U_\Omega = \omega r_i$. The rotation number is widely used in studies of rotating annular flows to provide ratios of the axial and rotational velocities. However, varying the imposed flow rate resulted in different N values for the same rotation rate of the inner cylinder. The present work aimed to report the effect of the axial and rotational flow control parameters separately. Thus, inner cylinder rotational velocities are symbolized as Ω_1 - Ω_5 for a clear representation of the results.

2.2. Numerical Details

A finite volume method-based commercial computational fluid dynamics code Simcenter Star-CCM+ was utilized to solve the governing equations, Reynolds Averaged Navier-Stokes Equations, of the transient incompressible flow. The Spatial derivatives are discretized by a second-order accurate central difference scheme. In the same way, a second-order implicit Euler scheme is used for time advancement. The SIMPLE algorithm is employed for velocity-pressure coupling. The no-

Table 2. *Summary of flow control parameters*

Axial velocity	Rotational velocity			*N*		
Re	**Ω**	**Re_Ω**	**Ta**	**For Re=10000**	**For Re=20000**	**For Re=30000**
10000 20000 30000	Ω_1	4704	2.16×10^7	0.94	0.47	0.31
	Ω_2	9446	8.71×10^7	1.89	0.94	0.63
	Ω_3	18854	3.47×10^8	3.77	1.89	1.26
	Ω_4	37784	1.39×10^9	7.55	3.77	2.52
	Ω_5	56600	3.13×10^9	11.32	5.66	3.77

Table 3. *Numerical details for different rotational velocities. Three values in each cell of the table correspond to the axial Reynolds number of 10,000, 20,000, and 30000, respectively*

	$N_r x N_\theta x N_z$	Δr_i^+	$r_i \Delta\theta^+$	Δz_i^+	CFL
Ω_1	64x140x127	0.34, 0.41, and 0.50	25, 31, and 38	32, 40, and 48	0.33, 0.43, 0.38
Ω_2	64x140x127	0.49, 0.54, 0.61	37, 41, and 46	47, 52, and 59	0.31, 0.34, and 0.35
Ω_3	97x180x192	0.33, 0.35, 0.36	40, 41, 53	58, 60, 63	0.26, 0.35, 0.22
Ω_4	97x180x192	0.60, 0.60, and 0.62	72, 73, and 89	105, 106, and 107	0.30, 0.30, 0.24
Ω_5	97x220x242	0.85, 0.85, and 0.86	84, 84, 85	117, 118, 118	0.30, 0.34, and 0.39
CFL: Courant-Friedrichs-Lewy					

slip condition is valid at all walls in the computational domain. A fixed tangential velocity component is assigned to the rotating inner cylinder. To ensure that the calculations were independent of the inflow conditions, periodic boundary conditions were applied in the axial direction. The same approach has been successfully implemented by several researchers to achieve fully developed flow conditions [12,15,21]. The results were checked with solutions in a relatively longer domain to ensure that the domain length was sufficiently long for large-scale turbulent structures.

Turbulence modeling is based on the low-Reynolds-number elliptic-blending Reynolds Stress Transport model (RSM). The model formulation was presented in Manceau and Hanjalić [43] and was not repeated here. The Reynolds stress model is free of the eddy viscosity assumption and accounts for the anisotropy of the Reynolds stress tensor. Thus, it can serve as a more realistic turbulence model for flows that includes swirling motion and rapid changes in the strain rate. It has been successfully applied to complex flow fields like vortex flows [44], rotating pipes [45], and TCP flows [19,40,46].

2.3. Grid Resolution

The computation grid was uniform in the axial and circumferential directions. In the wall-normal direction, the grid points were clustered near the inner and outer cylinders to achieve fine grid resolution near the walls. The first grid point was placed to keep the r^+ $\left(r^+ = u_\tau \Delta r/\upsilon\right)$ value below 1. The grid structure is detailed in Table 3. The mesh distribution between the cylinders can also be seen in Figure 2 (for 64x140x127 mesh). N_r , N_θ , and N_z donates the number of grid points in the radial, tangential, and axial directions, respectively. The grid structures presented in the table are obtained by conducting a systematic grid dependency study (which is presented in the following section). The initial grid was structured similarly to that in [12]. The number of grid points was refined for higher rotation rates because finer grids were needed in the axial direction to resolve the flow for increasing N [8]. Although the implemented implicit solution algorithm relieves the CFD restriction, relatively small time steps were selected to maintain the mean Courant-Friedrichs-Lewy (CFL) value (CFL = $U\Delta t/\Delta x$) around 1, to increase the accuracy. The maximum CFL value was 0.43 in all cases.

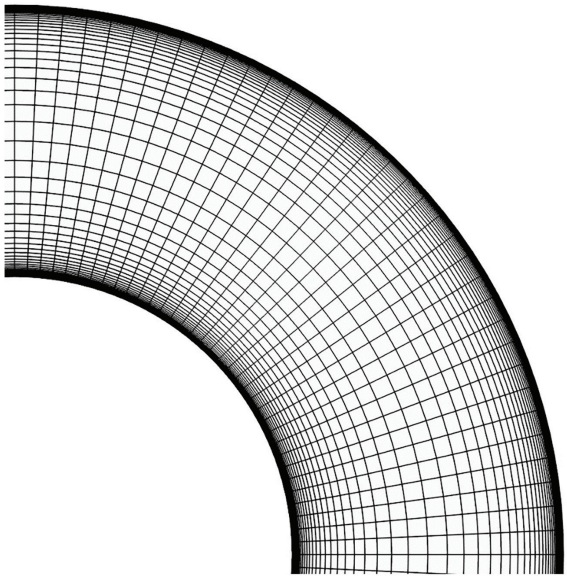

Figure 2. *Mesh distribution between the cylinders*

3. Numerical Accuracy Evaluation

The present calculations are compared with the experimental results of Escudier and Coulson [6] to validate the numerical methodology. Results of the validation case were obtained under the same conditions as the experiment, which are Re=7400 and Ω=126 rpm. This flow configuration resulted in a Taylor Number of Ta=8.75x10^5 and a rotation number N=0.25. Before comparing the numerical results with the experimental data, we studied the mesh dependency of the numerical predictions. To examine the impact of the mesh structure on the numerical results, the mesh distribution was changed separately in all directions, and variations in the results were observed. It's worthy of mention that the mesh density in the radial direction seems to have a greater influence on the tangential velocity distribution. Considering these findings and previous studies in the literature, the final mesh distribution was determined. Once the optimal mesh distribution was determined, the overall mesh count was parametrically changed in all directions to examine the mesh dependency of the numerical results (Figure 3). The validation case was selected for the mesh dependency study. Here, the medium mesh refers to the mesh distribution in the first row of Table 3 due to the similarity of the flow conditions. The coarse, medium, and fine mesh counts were 0.6, 1.14, and 2.55 million, respectively. When the results were examined, the coarse mesh structure was observed to underestimate the tangential velocity distribution along the radial gap, whereas

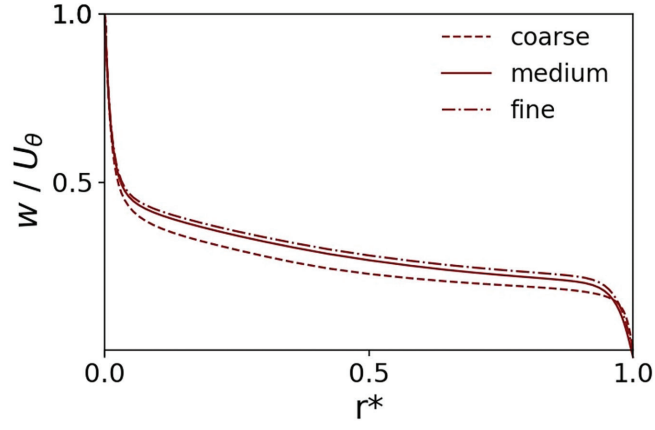

Figure 3. *The effect of mesh density on the numerical results*

the medium and fine mesh structures produced very similar results to each other. Therefore, considering computational time and accuracy together, the study was continued with a medium mesh structure.

Figure 4 compares the present results with those of Escudier and Coulson [6] for the mean axial and tangential velocity components. The predicted mean axial and tangential velocity profiles are non-dimensionalized by the bulk and inner cylinder rotational velocities, respectively. r^* represents the radial location $\left(r^* = r - r_i / s\right)$. The numerical predictions are in good agreement with the experimental ones. The velocity profiles in both the boundary layers and the core region were very similar to those obtained in the experiment. The predicted tangential velocity values are smoother and slightly higher than the measurements; nevertheless, the slope of the curve in the core region is successfully captured.

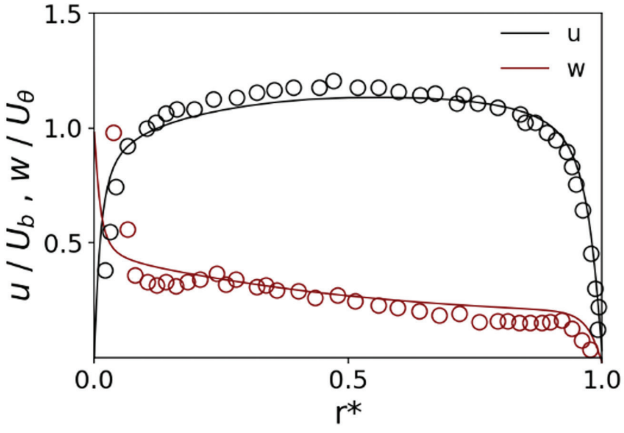

Figure 4. *Comparison of calculated mean velocity components (straight lines) with experimental data (symbols) along the radial direction*

The predicted axial and tangential turbulent fluctuations compared with the experimental data are plotted in Figure 5. The variation in the normal components of the Reynolds stress tensor along the radial direction was generally in good agreement with the measurements. In most parts of the radial distance, the tangential velocity fluctuation, w', calculations correspond well to the experimental results but exhibit a smoother profile. The turbulence intensity in the axial direction, u', is in the same tendency as in the experiment. The calculated turbulence levels in the core region and boundary layer along the outer cylinder were in the same magnitude as the measurements. However, some differences can be seen in the peak values of the fluctuations in the boundary layer along the inner cylinder. The same features were observed for near-wall velocity fluctuations in the RSM predictions of Poncet et al. [19] against the same measurements and the LES results of Chung and Sung [8] and DNS of Jung and Sung [10] against the experimental data of Nouri and Whitelaw [5]. Overall, it can be concluded that the flow field in the annular gap can be accurately predicted using the present numerical methodology.

4. Numerical Results

Detailed calculations were carried out for the parameter spaces summarized in Table 2. In Figure 6, we observe the distribution

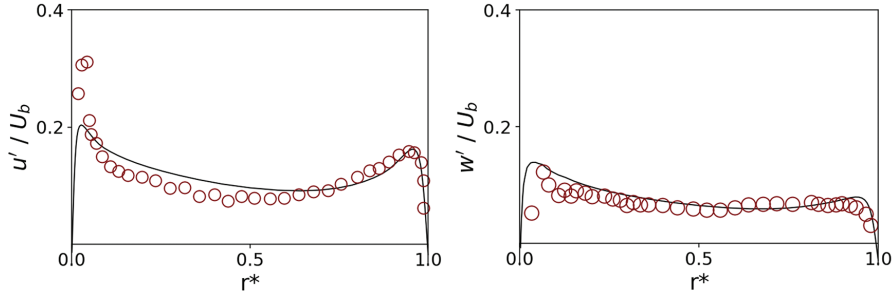

Figure 5. *Comparison of calculated axial and tangential velocity fluctuations (straight lines) and experimental data (symbols) along the radial direction*

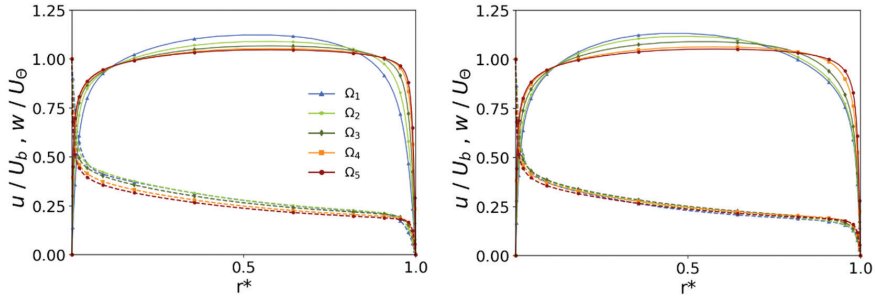

Figure 6. *Effect of rotation on distribution of mean axial (solid line) and tangential (dashed line) velocity components (left: Re=10000, right: Re=30000)*

of mean axial and tangential velocities normalized to the inlet bulk velocity and inner cylinder rotational velocity, respectively, across two different flow rates. Regardless of the axial velocity, all cases exhibit turbulent flow profiles. The increasing inner cylinder rotational speed flattens and slightly shifts the velocity profiles toward the outer wall, which is particularly evident at lower rotational speeds. Higher Reynolds numbers yield similar results. Rotation influences the normalized tangential velocity primarily near the inner cylinder, thinning the boundary layer and decreasing the slope of the core region profile, as previously pointed out by Poncet et al. [12]. It is worth noting that Poncet et al. [12] reported a solid body-like rotation in the core region with a decreasing slope of the tangential velocities toward zero. Their calculations consider a very narrow gap with a radius ratio of $r_1/r_2 = 8/9$. On the other hand, in the present results, the angular momentum is still almost constant, but the tangential velocity curves never show such a flatter profile in the center region. Similar variations in normalized tangential velocities can be observed in the LES results of Chung and Sung [8] with $r_1/r_2 = 0.5$. At higher axial flow rates, changes in the rotational speed have less impact on the tangential velocity profiles because of the limited rotation number variation. Increasing the flow rate prioritizes the axial velocity, diminishing the influence of rotation under the same rotational parameters.

The influence of the imposed flow rate on the distribution of the mean velocity components can be seen in Figure 7, for the highest and lowest rotational speeds of the inner cylinder. The axial velocity profiles showed slight deviations with flow rate variations. An increase in Re reverses the effect of rotation, and the axial velocity profiles start to have lower gradients near the outer stationary wall at low rotational speed (Figure 7-left). The effect of the imposed flow rate on the tangential velocity is more apparent. Tangential velocity values exhibit a progressive decrease nearly in the entire flow field with increasing Re. As stated by Nouri and Whitelaw [5], increasing the axial flow rate limits the penetration of the influence of rotation through the inner parts of the annular gap. For the higher rotational speed (Figure 7-right), the imposed flow rate seems to have no considerable influence on the mean velocity components. It is worth noting that N varies in the range of 0.31-0.94 for Ω_1 and 3.77-11.32 for Ω_5. Even when the change in N was larger, the case with higher rotation was almost not affected by the variation in the imposed flow rate. It can be concluded that rotation determines the flow field; thus, the influence of the imposed flow rate on the mean velocity components diminishes, as the Ω increases.

The response of low and high rotational speeds to changes in the axial flow rate, regardless of the variation in N, prompts an examination of the mean velocity balance across the annular gap (Figure 8). Cross-stream velocity remains nearly zero across all cases, while the normalized axial velocity exhibits minimal variation with changing flow conditions. Notably, variations in the rotational and/or axial flow control parameters primarily affect the tangential velocity distribution. At low rotational speeds (Figure 8a), the axial velocity dominates the flow field, with the velocity magnitudes decreasing from the axial to the tangential to the cross-stream components. Increasing the rotational speed (in the meantime N) augments the tangential velocity, particularly in the first half of the radial distance (where $0<r<0.5$). At low Re, the same amount of change in the rotational speed results in higher N, thereby enhancing the tangential velocity. As previously mentioned for the numerical results in Figure 6, axial flow limits the penetration of the effect of the rotation through the inner parts of the flow field for the same rotational speed (e.g. Figure 8b, f, j).

Another remarkable feature of the velocity distributions for different axial/rotational velocity pairs is the balance near the inner rotating cylinder. After a certain value of N (approximately $1.89<N<2.52$ in the investigated range), the tangential velocity becomes dominant in the near region of the inner cylinder. These findings provide some insights into Figure 7, where the

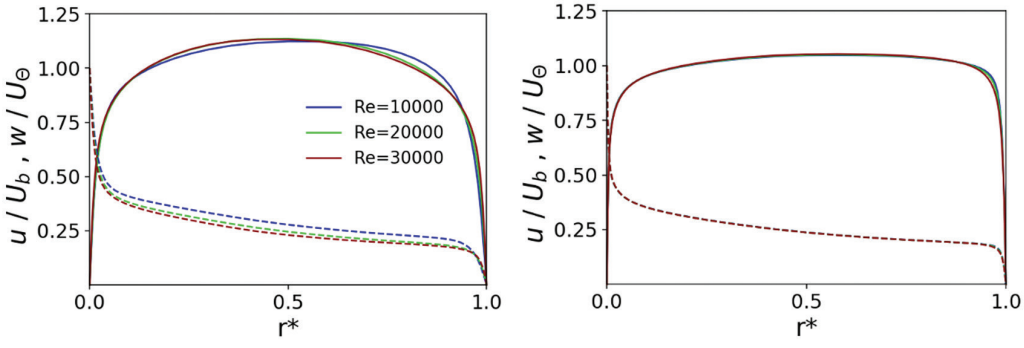

Figure 7. *Effect of axial velocity on distribution of mean velocity components. dashed: mean axial velocity; Straight line: mean tangential velocity (left:Ω_1, right: Ω_5)*

higher rotation case shows minimal sensitivity to changes in the imposed flow rate despite larger variations in N. When the rotational speed of the inner cylinder is relatively low (e.g. $\Omega_1$or Ω_2), axial velocity is dominating the flow field (see Figure 8a, e, i). On the other hand, beyond a certain N value, the tangential velocity becomes dominant near the inner cylinder, thereby influencing the flow-field balance. This dominance persisted even with varying Re (see Ω_5 at Figure 8d, h, l). The results thus far suggest that beyond a threshold N value, rotation dominates near the inner cylinder, and the contribution of rotation becomes

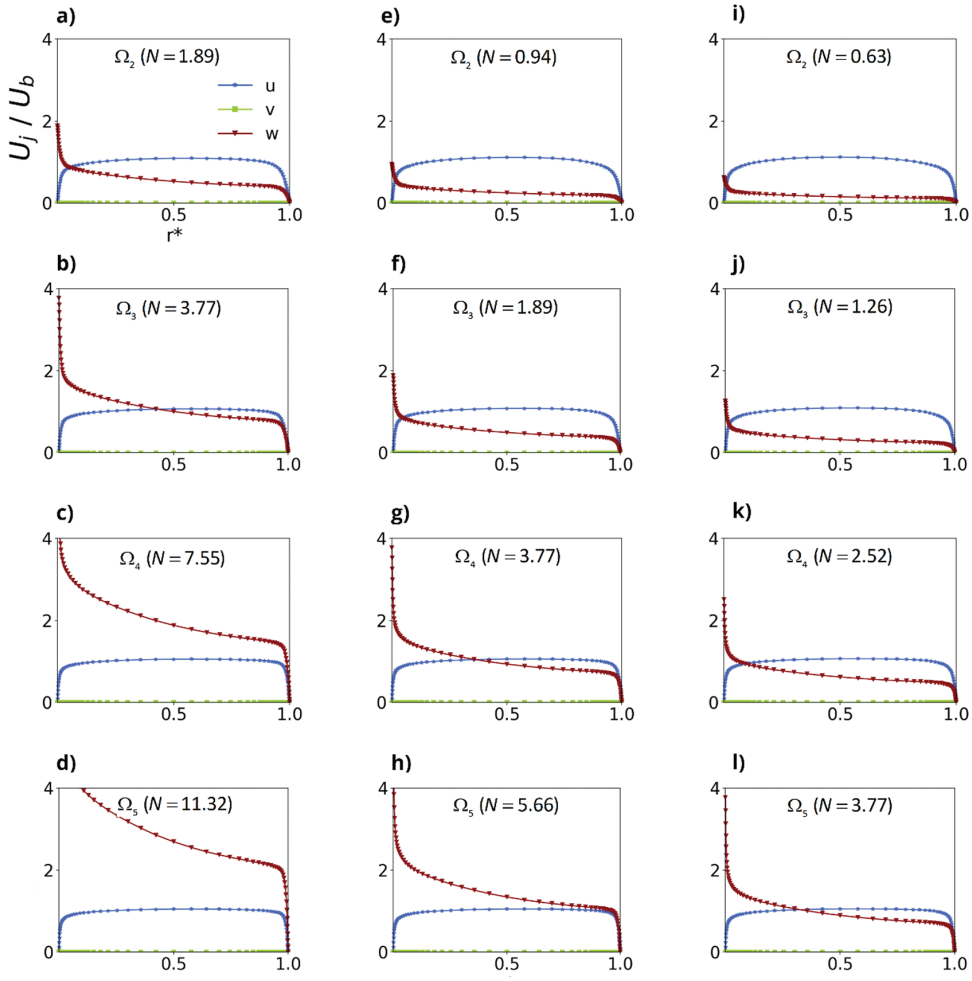

Figure 8. *Distribution of mean velocity components normalized by Ub along the radial gap (left column: Re=10000, middle: Re=20000, right: Re=30000)*

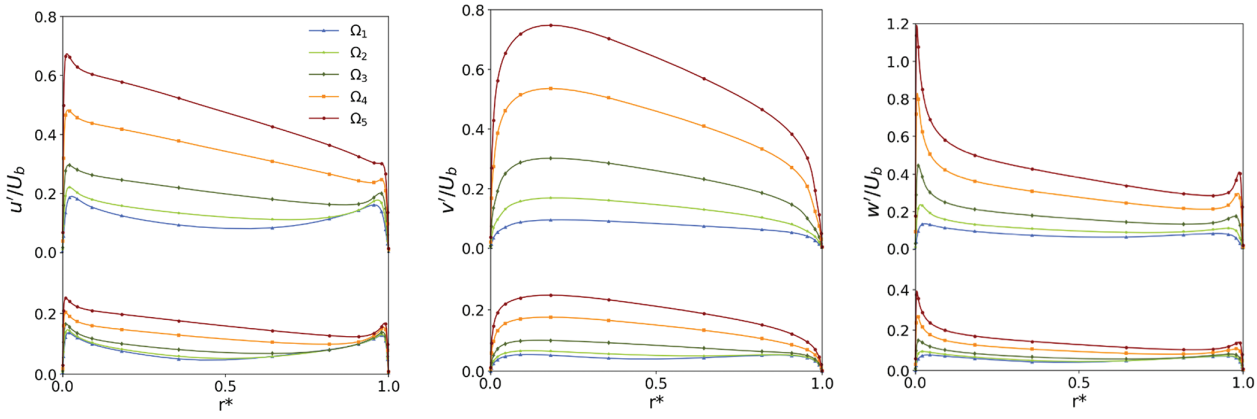

Figure 9. *Effect of rotation on distribution of normal components of Reynolds stress tensor (lower: Re=30000, lifted: Re=10000)*

superior, making mean flow variables less sensitive to changes in the axial flow rate within the specified N range.

Figure 9 presents the effect of rotation on the distribution of normal components of the Reynolds stress tensor. The inner cylinder rotation triggers turbulence, which results in the rapid growth of all turbulence intensities as the rotational speed increases. Turbulence enhancement is limited at high Re. *u*' stress shows a profile with a peak centered at the boundary layer. The magnitude of the *u*'stress in the core region increased with the rotational speed; nevertheless, the peak values were still in the near region of the inner cylinder. *w*' stress retains the general behavior with high values in the boundary layers in all cases. The cross-stream component of the Reynolds stress tensor, *v*', distinctly has higher values in the core region and vanishes toward the walls. All profiles of turbulence intensities are highly asymmetric, which is attributed to the destabilizing effect of centrifugal forces, as noted by Chung and Sung [8]. The asymmetry becomes more apparent with the increase in Ω , akin to similar studies in the literature with the same radius ratio [8,21]. However, Poncet et al. [12] predicted notably weaker asymmetry with a narrow-gap annulus with a radius ratio of $r_i/r_o = 8/9$ within the range of rotational parameters 1.49<N<6.71. Despite the low curvature effect, it can be attributed to the close proximity of the rotating and stationary walls in narrow gap systems.

Figure 10 shows the effect of the axial flow on the distribution of normal stresses at the highest and lowest inner cylinder rotation speeds. In general, an increase in the axial flow rate suppresses the turbulence in the entire flow field. This effect is clearer near the inner cylinder at high rotation rates. The axial flow independence of higher rotation rates noted earlier in the mean velocity profiles (see Figure 7) is not observed for the turbulence variables. The turbulence stresses still exhibit a dependence on both the axial flow rate and the system rotation. The change in the imposed flow rate alters the turbulence stress components in a similar way for low and high rotation speeds of the inner cylinder, except that the results at higher rotation rates vary over a wider range of values.

The velocity profiles in the boundary layer along the inner cylinder are plotted against the law of the wall in Figure 11. It can be seen that rotation causes no significant change in the velocities of the viscous sublayer. However, the profiles in the buffer and log-law regions differed considerably from the wall law. Furthermore, the level of this discrepancy depends

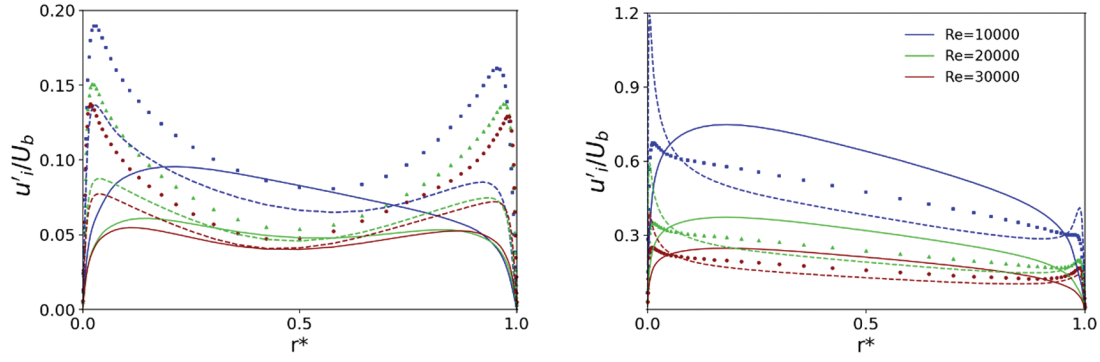

Figure 10. *Effect of axial flow on normal components of Reynolds stress tensor. Symbols donate u', straight line v', and dashed line w' (left: Ω_1, right:Ω_5)*

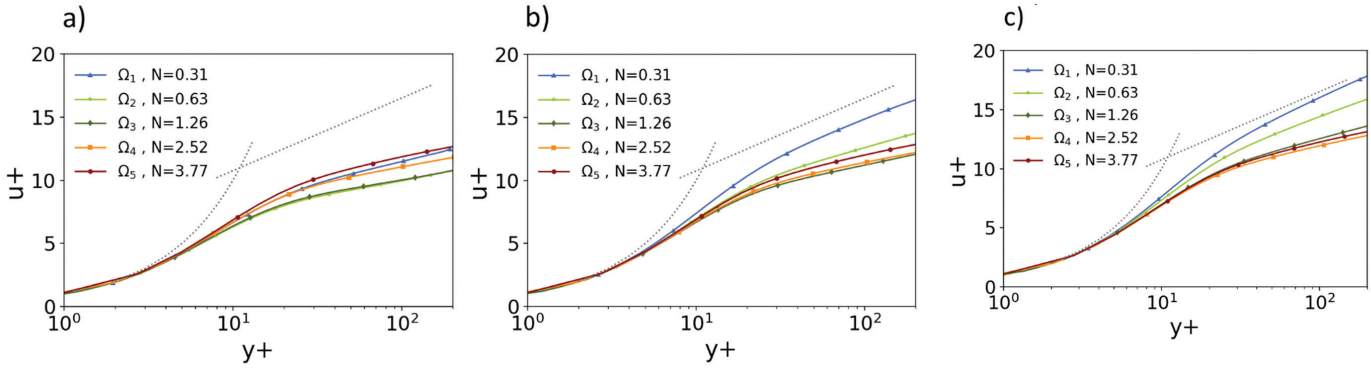

Figure 11. *Boundary layer velocity distribution under the law of the wall (a: Re=10000, b: Re=20000, c: Re=30000)*

on the value of N. For instance, in Figure 11a, velocities in the boundary layer diverge from the standard log-law as the rotational speed of the inner cylinder increases up to Ω_2 . However, a further increase in rotation shifts the profiles closer to that of the law of the wall. The value of N at which the effect of rotation is reversed is 1.89<N<2.52 in the investigated range. This value also coincides with the range where the mean tangential velocity dominates the near-wall region of the inner rotating cylinder at Figure 8. Note that the increment rate of the rotational speed of the inner cylinder causes the values N to jump from one value to another, and determining intermediate values requires many more cases to solve. This is the reason why the present study suggests ranges instead of exact values of N. The results are in accordance with those of other studies in the literature. Schneider et al. [21] and Chung and Sung [8] reported an increasing discrepancy between the boundary layer velocity profiles and those of the law of the wall with increasing N from 0 to 0.858. However, in the LES results of Poncet et al. [12], the velocities in the logarithmic region approached the log-law with increasing N from 2.24 to 6.71.

The effect of the axial flow on the law of the wall for boundary layer velocity is shown in Figure 12. At low cylinder rotation, an increase in the axial flow rate suppresses the influence of rotation and decreases the discrepancy of the velocity profiles with the log-law (see Figure 12-left). However, the axial flow seems to have no considerable effect on the boundary layer velocity profiles at high rotational speeds, even though N varies in a wider range (see Figure 12-right). Note that the mean velocity profiles in Figure 7 were also nearly unaffected by the axial flow at high system rotation. Here, the same feature that is explained in Figure 8, the superior value of the tangential velocity near the rotating wall, which is thought to be the reason why the effect of the imposed flow is considerably limited in Figure 12-right.

5. Conclusion

This study conducted a numerical investigation of a fully developed turbulent flow within a concentric annular channel. A RSM-based numerical procedure was employed to examine the effects of the inner wall rotational velocity and imposed axial flow rate on the flow dynamics. The numerical predictions were first validated against experimental data by Escudier and Coulson [6]. Subsequently, various flow control parameters were investigated. This research focused on the behavior of the TCP system at high Reynolds numbers. The key findings are summarized below:

• The influence of flow control parameters on the mean flow variables differed between high and low system rotation. At higher rotational speeds, the mean flow variables are nearly independent of the changes in the imposed flow rate, regardless of the rotation number (N) variation.

• The balance between the mean velocity components across the radial gap exhibits a significant dependence on both rotation and the imposed axial flow. As expected, increasing rotation increased the tangential velocity, particularly in the first half of the radial gap near the inner wall. Beyond a certain value of N, the tangential velocity becomes dominant in the flow field between the inner wall and core region. At even higher N values, the flow field is likely to be more dominated by the contribution of rotation. This phenomenon explains the observed independence of mean flow features from axial flow at high rotational speeds.

• In general, the imposed flow and rotation have opposing effects on the turbulence behavior. Inner wall rotation significantly enhanced the turbulence statistics, whereas axial flow suppressed the destabilizing effect of rotation. Unlike the mean flow variables, the turbulence intensities decreased with increasing axial flow rate at any rotational speed.

• Rotation has a non-monotonic effect on the agreement of the boundary layer velocity profiles with the law of the wall. As the rotational speed increases, the discrepancy of the boundary-layer velocities with the log law initially increases but then decreases. The rotation rate at which this behavior

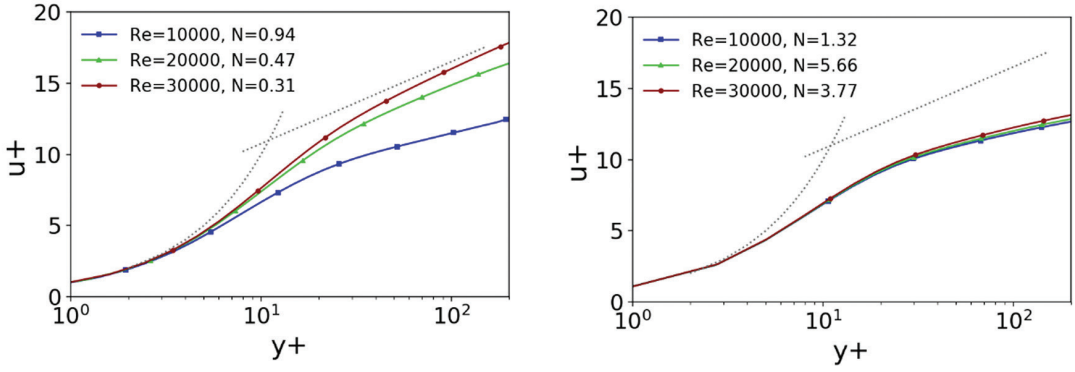

Figure 12. *Effect of axial flow on the velocity distribution in the boundary layer (left:* Ω_1*, right:*Ω_5*)*

shift coincides with the range in which the tangential velocity dominates the flow field.

These results provide valuable insights into the complex interplay between rotation and axial flow in TCP systems. This knowledge can be used to optimize the design and operation of various engineering applications.

Authorship Contributions

Concept Design: T. Çoşgun, N. Vardar, Data Collection or Processing: T. Çoşgun, Analysis or Interpretation: T. Çoşgun, Literature Review: T. Çoşgun, N. Vardar, Writing, Reviewing and Editing: T. Çoşgun, N. Vardar.

Funding: The authors received no financial support for the research, authorship, and/or publication of this article.

References

[1] D. L. Cotrell, "Flow Between a Cylinder and a Rotating Coaxial Cylinder, Axisymmetric Shaft With Axially-Periodic Radius Variation, or Screw," University of Illinois at Urbana-Champaign, vol. 112, pp. 153-161, Jun 2003.

[2] M. Bilson, and K. Bremhorst, "Direct numerical simulation of turbulent Taylor-Couette flow". *Journal of Fluid Mechanics,* vol. 579, pp. 227-270, May 2007.

[3] S. Grossmann, D. Lohse, and C. Sun, "High-Reynolds number taylor-couette turbulence". *Annual Review of Fluid Mechanics,* vol. 48, pp. 53-80, 2016.

[4] M. Fénot, Y. Bertin, E. Dorignac, and G. Lalizel, "A review of heat transfer between concentric rotating cylinders with or without axial flow". *International Journal of Thermal Sciences,* vol. 50, pp. 1138-1155, Jul 2011.

[5] J. M. Nouri, and J. H. Whitelaw, "Flow of newtonian and non-newtonian fluids in a concentric annulus with rotation of the inner cylinder," *Journal of Fluids Engineering,* vol. 116, pp. 821-827, Dec 1994.

[6] M. P. Escudier and I. W. Gouldson, "Concentric annular flow with centerbody rotation of a Newtonian and a shear-thinning liquid". *International Journal of Heat and Fluid Flow*, vol. 16, pp. 156-162, Jun 1995.

[7] S. Chung, G. Rhee, and H. Sung, "Direct numerical simulation of turbulent concentric annular pipe flow: Part 1: Flow field". *International Journal of Heat and Fluid Flow*, vol. 23, pp. 426-440, 2002.

[8] S. Y. Chung, and H. J. Sung, "Large-eddy simulation of turbulent flow in a concentric annulus with rotation of an inner cylinder". *International Journal of Heat and Fluid Flow,* vol. 26, pp. 191-203, 2005.

[9] N. S. Liu, and X. Y. Lu, "Large eddy simulation of turbulent flows in a rotating concentric annular channel". *International Journal of Heat and Fluid Flow,* vol. 26, pp. 378-392, Jun 2005.

[10] S. Y. Jung, and H. J. Sung, "Characterization of the three-dimensional turbulent boundary layer in a concentric annulus with a rotating inner cylinder". *Physics of Fluids,* vol. 18, 2006.

[11] M. Hadžiabdić, K. Hanjalić, and R. Mullyadzhanov, "LES of turbulent flow in a concentric annulus with rotating outer wall". *International Journal of Heat and Fluid Flow*, vol. 43, pp. 74-84, Oct 2013.

[12] S. Poncet, S. Viazzo, and R. Oguic, "Large eddy simulations of Taylor-Couette-Poiseuille flows in a narrow-gap system". *Physics of Fluids*, vol. 26, pp. 1070-6631, Oct 2014.

[13] Y. Yamada, "Resistance of a Flow through an Annulus with an Inner Rotating Cylinder". *Bulletin of JSME*, vol. 5, pp. 302-310, 1962.

[14] M. Manna, and A. Vacca, "Torque reduction in Taylor-Couette flows subject to an axial pressure gradient". *Journal of Fluid Mechanics,* vol. 639, pp. 373-401, Nov 2009.

[15] A. Ohsawa, A. Murata, and K. Iwamoto, "Through-flow effects on Nusselt number and torque coefficient in Taylor-Couette-Poiseuille flow investigated by large eddy simulation". *Journal of Thermal Science and Technology,* vol. 11, pp. JTST0031-JTST0031, Jun 2016.

[16] N. S. Woo, Y. J. Kim, and Y. K. Hwang, "Experimental study on the helical flow in a concentric annulus with rotating inner cylinder". *Journal of Fluids Engineering*, vol. 128, pp. 113-117, 2006,

[17] Y. C. Chong, D. A. Staton, M. A. Mueller, and J. Chick, "An experimental study of rotational pressure loss in rotor-stator gap". *Propulsion and Power Research*, vol. 6, pp. 147-156, Jun 2017.

[18] S. Huang, and C. H. Chun, "A numerical study of turbulent flow and conjugate heat transfer in concentric annuli with moving inner rod". *International Journal of Heat and Mass Transfer,* vol. 46, pp. 3707-3716, Sep 2003.

[19] S. Poncet, S. Haddadi, and S. Viazzo, "Numerical modeling of fluid flow and heat transfer in a narrow Taylor-Couette-Poiseuille system". *International Journal of Heat and Fluid Flow*, vol. 32, pp. 128-144, 2011.

[20] A. Aubert, S. Poncet, P. Le Gal, S. Viazzo, and M. Le Bars, "Velocity and temperature measurements in a turbulent water-filled Taylor-Couette-Poiseuille system". *International Journal of Thermal Sciences*, vol. 90, pp. 238-247, 2015.

[21] M. Schneider, B. A. Younis, and B. Weigand, "Large-eddy simulations of flow and heat transfer in heated concentric annulus with inner cylinder rotation". *International Journal of Heat and Mass Transfer,* vol. 114, pp. 1248-1262, Apr 2017.

[22] J. M. Lopez, F. Marques, and M. Avila, "Conductive and convective heat transfer in fluid flows between differentially heated and rotating cylinders". *International Journal of Heat and Mass Transfer,* vol. 90, pp. 959-967, Nov 2015.

[23] J. Kaye, and E. C. Elgar, "Modes of adiabatic and diabatic fluid flow in an annulus with an inner rotating cylinder". *Transactions of the ASME*, vol. 80, pp. 753-765, Apr 1958.

[24] K. M. Becker, and J. Kaye, "Measurements of diabatic flow in an annulus with an ınner rotating cylinder". *ASME Journal of Heat and Mass Transfer,* vol. 84, pp. 97, May 1962.

[25] D. I. Takeuchi, and D. F. Jankowski, "A numerical and experimental investigation of the stability of spiral poiseuille flow". *Journal of Fluid Mechanics,* vol. 102, pp. 101-126, Jan 1981.

[26] Z. H. Gu, and T. Z. Fahidy, "Characteristics of Taylor vortex structure in combined axial and rotating flow". *The Canadian Journal of Chemical Engineering,* vol. 63, pp. 710-715, Oct 1985.

[27] M. Molki, K. N. Astill, and E. Leal, "Convective heat-mass transfer in the entrance region of a concentric annulus having a rotating

inner cylinder". *International Journal of Heat and Fluid Flow*, vol. 11, pp. 120-128, Jun 1990.

[28] R. M. Lueptow, A. Docter, and K. Min, "Stability of axial flow in an annulus with a rotating inner cylinder". *Physics of Fluids*, vol. 4, pp. 2446-2455, Nov 1992.

[29] S. T. Wereley, and R. M. Lueptow, "Velocity field for Taylor-Couette flow with an axial flow". *Physics of Fluids*, vol. 11, pp. 3637-3649, 1999.

[30] J.Y. Hwang and K.S. Yang, "Numerical study of Taylor-Couette flow with an axial flow". *Computers & Fluids,* vol. 33, pp. 97-118, Jan 2004.

[31] S. Y. Jung, and H. J. Sung, "Large-eddy simulation of turbulent mixed convection in a vertical annulus with a rotating inner cylinder". *Journal of Turbulence*, vol. 8, pp. N5, Jan 2007.

[32] T. M. Jeng, S. C. Tzeng, and C. H. Lin, "Heat transfer enhancement of Taylor-Couette-Poiseuille flow in an annulus by mounting longitudinal ribs on the rotating inner cylinder". *International Journal of Heat and Mass Transfer,* vol. 50, pp. 381-390, Jan 2007.

[33] M. Fénot, E. Dorignac, A. Giret, and G. Lalizel, "Convective heat transfer in the entry region of an annular channel with slotted rotating inner cylinder". *Applied Thermal Engineering,* vol. 54, pp. 345-358, May 2013.

[34] C. Leclercq, B. Pier, and J. F. Scott, "Temporal stability of eccentric taylor-couette-poiseuille flow". *Journal of Fluid Mechanics*, vol. 733, pp. 68-99, Sep 2013.

[35] K. R. Anderson, J. Lin, C. McNamara, and V. Magri, "CFD study of forced air cooling and windage losses in a high speed electric motor". *Journal of Electronics Cooling and Thermal Control,* vol. 5, pp. 27-44, Jan 2015.

[36] W. Abassi, F. Aloui, S. B. Nasrallah, and J. Legrand, "Use of the PIV and electrochemical techniques to experimentally characterize the couette-taylor-poiseuille flow ınstabilities". *Journal of Applied Fluid Mechanics,* vol. 9, Special Issue 1, pp. 59-68, 2016.

[37] N. Tilton, and D. Martinand, "Taylor-Couette-Poiseuille flow with a weakly permeable inner cylinder: Absolute instabilities and selection of global modes". *Journal of Fluid Mechanics*, vol. 849, pp. 741-776, Aug 2018.

[38] G. Luo, Z. Yao, and H. Shen, "Mechanism of pressure oscillation in Taylor-Couette-Poiseuille flow with abruptly contracting and expanding annular gap". *Physics of Fluids*, vol. 31, pp. 075105, Jul 2019.

[39] A. Nouri-Borujerdi and M. E. Nakhchi, "Prediction of local shear stress and heat transfer between internal rotating cylinder and longitudinal cavities on stationary cylinder with various shapes". *International Journal of Thermal Sciences,* vol. 138, pp. 512-520, Apr 2019.

[40] S. Gokul, and M. Deepu, "Fluid flow and heat transfer in an annulus with ribs on the rotating ınner cylinder surface". *International Journal of Heat and Mass Transfer*, vol. 12, 041026, Aug 2020.

[41] I. Mochalin, E. Shi-Ju, D. Wang, and J.-C. Cai, "Numerical study of heat transfer in a Taylor-Couette system with forced radial throughflow". *International Journal of Thermal Sciences*, vol. 147, pp. 106142, Jan 2020.

[42] A. Gavrilov, and Y. Ignatenko, "Numerical simulation of taylor-couette-poiseuille flow at re = 10,000". *Fluids*, vol. 8, pp. 1-17, 2023.

[43] R. Manceau, and K. Hanjalić, "Elliptic blending model: A new near-wall Reynolds-stress turbulence closure". *Physics of Fluids,* vol. 14, pp. 744-754, Feb 2002.

[44] S. Lardeau, and R. Manceau, "Computations of complex flow configurations using a modified elliptic-blending Reynolds-Stress model". *10th International ERCOFTAC Symposium on Engineering Turbulence Modelling and Measurements*, 2014.

[45] N. Ashton, J. Davis, and C. Brehm, "Assessment of the elliptic blending reynolds stress model for a rotating turbulent pipe flow using new DNS data". *American Institute of Aeronautics and Astronautics (AIAA),* Jun 2019.

[46] J. L. V. Neto, A. L. Martins, A. S. Neto, C. H. Ataíde, and M. A. S. Barrozo, "CFD applied to turbulent flows in concentric and eccentric annuli with inner shaft rotation". *The Canadian Journal of Chemical Engineering,* vol. 89, pp. 636-646, Aug 2011.